Utilizing QCM-D To Characterize the Adhesive Mucilage Secreted by Two Marine Diatom Species in-Situ and in Real-Time

Paul J. Molino,[†] Oliver M. Hodson,[†] John F. Quinn,[‡] and Richard Wetherbee*[,†]

School of Botany, and Centre for Nanoscience and Nanotechnology, Department of Chemical and Biomolecular Engineering, The University of Melbourne, Parkville, Victoria 3010, Australia

Received June 13, 2006; Revised Manuscript Received August 1, 2006

The quartz crystal microbalance with dissipation monitoring (QCM-D) was used to monitor the deposition of adhesive extracellular polymeric substances (EPS) employed by the marine biofouling diatoms *Craspedostauros australis* Cox and *Amphora coffeaeformis* Cleve during initial adhesion and subsequent motility. Upon injection into the QCM chamber, initial negative frequency (*f*) shifts and positive dissipation (*D*) shifts were measured that correlated to cells impacting and adhering to the QCM sensor surface. Following this "initial adhesion" response, *f* continued to decrease while *D* increased logarithmically. Rather than the result of any cell morphological alterations at the substrate surface, the shifts were correlated to the time-dependent deposition of EPS upon the substrate surface as a result of cellular motility, or gliding. Experiments utilizing comparable cell concentrations of the diatom species *C. australis* and *A. coffeaeformis* revealed significant differences between the parameter responses recorded, where *A. coffeaeformis* produced Δf and ΔD values of −32 Hz and 6.6, and *C. australis* produced values of −82 Hz and 42, respectively, after 20 h post-inoculation. The viscoelastic properties of the adhered EPS adlayer from both species were examined via a $\Delta f/\Delta D$ plot, providing reproducible signature "ratio" values for each species that likely correlate to differences in EPS interactions with the substrate that may be associated directly to differences in the fouling potential of the two species. There is a distinct lack of knowledge regarding the chemical nature of the adhesive polymers engaged, and few quantitative techniques are applicable to the study of diatom EPS. We propose that QCM-D may be a useful tool in identifying differences in the EPS employed by diatoms of different fouling potential.

Introduction

The quartz crystal microbalance (QCM) is a versatile instrument with applications in a wide variety of fields (for reviews, see O'Sullivan and Guilbault,[1] Marx[2]). The technique was pioneered by Sauerbrey,[3] who first described the mass sensing capabilities of piezoelectric quartz crystals; thereafter, QCM became an effective tool in analytical chemistry where it was used for measuring the mass bound to the quartz crystal surface from the gas phase.[4] The development of QCM in liquids allowed for the measurement of interactions at the solution−surface interface.[5,6] Nomura and Okuhara[5] observed changes in the oscillation frequency of the crystal dependent upon the density and viscosity of the contacting liquid. QCM in solution facilitated studies in electrochemistry,[7,8] immunology,[9−11] and cell biology, where they were introduced as primitive sensors for cell attachment and growth.[12−14] Researchers soon developed the instrument to measure not only the adsorbed mass upon the surface in *f* (frequency), but also the viscoelastic properties of the adhered layer using the dissipation factor, *D*, and the comparable *Q* factor.[15−17] These new parameters were promptly applied to the investigation of cellular adhesion,[18,19] and several researchers have since utilized the QCM to study cellular interactions at the solution−surface interface.[20−27]

Wegener et al.[20] utilized the QCM to monitor the adhesion and spreading of several mammalian cell lines, describing the maximum frequency shifts dependent upon the number of cells seeded onto the crystal surface, where the nature of these shifts was determined to be cell species dependent. Zhou et al.[21] employed the QCM as a continuous monitoring tool for endothelial cell (EC) surface attachment and growth. Along with reporting *f* shifts proportional to cell densities at the electrode surface, they also identified a time-dependent increase in ΔR values (i.e., motional resistance; related to the dissipation factor *D*) that were correlated to initial cell attachment and ensuing augmentation of cell cytoskeletal morphology. Subsequent work by this group[28] utilized the known microtubule binding drug nocodazole to trigger microtubule depolymerization in endothelial cells adhered to the QCM surface. Upon the introduction of nocodazole, negative shifts in *f* and positive shifts in *R* were measured and, through comparable light microscopy simulation experiments, were correlated with changes in cell morphology that reduced cell−cell contact, and subsequently cell contact with the substrate.

The earliest investigators who explored QCM-based cellular applications quickly realized that a cellular monolayer upon the electrode surface failed to act as an elastic mass, and therefore rendered the Sauerbrey equation, used to determine the adsorbed mass upon the crystal surface, inapplicable.[18] Analysis of QCM data generated from cellular-based studies required a detailed understanding of the interactions between the cells and the substrate surface. Wegener et al.[29] studied the adhesion and spreading of several mammalian cell lines, applying various treatments to probe the nature of the cellular contributions to the response parameters recorded. They concluded that only cellular components and compartments involved in specific

* To whom correspondence should be addressed. E-mail: richardw@unimelb.edu.au.

[†] School of Botany.

[‡] Centre for Nanoscience and Nanotechnology.

10.1021/bm0605661 CCC: $33.50
Published on Web 10/03/2006

integrin-mediated cellular adhesion and therefore in close proximity to the substrate surface are recorded, with the extracellular matrix (ECM), actin cytoskeleton, and the basal membrane−substrate separation distance all important contributing components.

While significant progress has been achieved in the study of mammalian cells for applications in biomedical research, surprisingly few studies have been directed toward applications in other areas, including those pertinent to the adhesion of marine microorganisms to man-made surfaces (i.e., biofouling). Recently, QCM has been utilized to study the adsorption behavior and cross-linking of polymers extracted from adhesives utilized by the Blue Mussel *Mytilus edulis*[30,31] and the marine alga *Fucus serratus*,[32] but as yet no work has been attempted using live eukaryotic cells that employ extra-cellular adhesives during adhesion and motility. Here, we explore QCM as an instrument with which to study the interactions between the adhesive mucilage secreted by marine diatoms and the substrate surface, in-situ and in real-time.

Diatoms (Bacillariophyceae) are a diverse group of algae that are ubiquitous in aquatic habitats. They have a distinctive morphology that includes a highly ornamented, siliceous cell wall plus associated organic layers and coverings that define the diatom frustule. The silica walls of pennate diatoms include an elongated slit termed a "raphe" through which adhesive mucilage is secreted to attach cells to the substratum. Because the silica walls are normally quite thick, the distance between the site of adhesive secretion at the plasma membrane and its adherence to the substratum can be considerable when compared to mammalian cells (in the species studied here, up to a micrometer or more). Most pennate species are defined by their ability to adhere and then "glide" over a surface, a process that deposits a mucilaginous trail upon the substrate surface (for review, see Edger and Picket-Heaps,[33] Hoagland,[34] Wetherbee et al.[35]). The secreted trail material accumulates to form a layer, which for diatoms can comprise a major component of the problematic biofoul layer found on artificial surfaces placed in the marine environment.

Although a number of studies have explored the effect surface chemistry has on the adhesion strength and motility behavior of a range of fouling diatoms,[36−38] the biochemistry of diatom extracellular polymeric substances (EPS) is still largely unknown, including the nature of the interaction with the substrate. Atomic force microscopy (AFM) has gone some way to characterize the tensile properties of the adhesive strands secreted from the raphes' of a number of diatom species.[39,40] In this report, we utilize the QCM-D technique to study the interactions between secreted EPS and the substratum during initial adhesion and motility for two fouling diatom species.

Materials and Methods

Algal Cell Culture. *Craspedostauros australis* Cox was collected from Western Port Bay, Victoria, Australia (Figure 1a). *Amphora coffeaeformis* Cleve was collected from the Defence Science and Technology Organization (DSTO) Maritime Testing Facility at Williamstown, Victoria, Australia (Figure 1b). *A. coffeaeformis* was chosen because it is known as a notorious ubiquitous bio-fouler; conversely, *C. australis* was chosen for examination as it is regarded as a relatively weak bio-fouling diatom species. Cells were isolated and maintained in 200 mL Pyrex conical flasks with sterile K-medium containing silicates[41] at 16 °C under Sylvania 15W Cool White fluorescent lamps with a daily 14:10 h light/dark cycle. To inhibit any potential bacterial contamination, cultures for QCM analysis and cell staining were treated with the combined use of 0.1 mg mL^{-1} streptomycin sulfate and 100 units mL^{-1} sodium penicillin G while in a log-phase of growth for a duration of 24 h, and thereafter cells were rinsed with sterile K-medium 24 h prior to use.

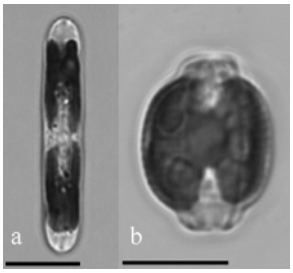

Figure 1. Transmission mode SLCM images of *C. australis* (a) and *A. coffeaeformis* (b). Scale bars, 13 μm (a) and 11 μm (b).

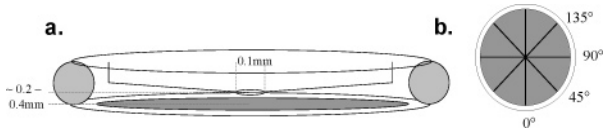

Figure 2. (a) Schematic of Q-Sense axial flow chamber (QAFC301). Diameter of fluid injection port is 0.1 mm, sitting directly above the QCM sensor. The sensor rests upon an O-ring at ~0.2−0.4 mm from injection point. Chamber volume is ~80 μL. (b) Image paths used to sample cell concentration upon the sensor surface after QCM analysis (area sampled ~23% of total electrode area).

Microscopic Analysis of Trail Formation. Glass microscope slides (Sail brand − 26 × 76 mm) were placed in plastic Petri dishes (90 × 14 mm) where a 1 mL aliquot of K-medium with suspended cells was placed upon the slide and allowed to settle for 5 min. Approximately 20 mL of K-medium was then added to the dish until slides were fully immersed and returned to the culture chamber. Slides were systematically removed from their dish, and approximately 2 mL of Stains-All (0.1 g of "Stains All" [Sigma, St. Louis, MO] in 100 mL of formamide) was added to the slide surface and left for several minutes. Slides were gently rinsed in sterile K-medium, and a cover slip (Marienfeld − 22 × 22 mm) was placed upon the slide and sealed with wax. Cells were stained following incubation times of 30 min, 1 h, 4 h, and 20 h. Images of cells and mucilaginous trails were obtained using light microscopy (Leica BH2) with a Leica DC 300F digital camera, and a Leica DM IRB inverted scanning laser microscope in reflection mode (488 nm laser) using a 63×/1.4 NA oil immersion lens.

QCM Analysis. Cells were harvested at the penultimate hour of their light cycle to limit any disruption to the cells accustomed daily cycle on injection to the dark QCM chamber. Cells were removed from culture flasks by applying light pressure to the flask surface using a disposable plastic pipet. Media containing dislodged cells were transferred to 10 mL Falcon tubes, with cells pelleted using a hand driven, bench-clamped centrifuge (Hettich 1101, CT). The supernatant was decanted off with the cells resuspended in fresh sterile K-medium up to the desired cell concentration.

QCM measurements were taken using a Q-Sense QCM-D300 with a Q-Sense axial flow cell (QAFC301) (Q-Sense AB, Västra Frölunda, Sweden) (Figure 2a). The QCM sensor was an A-T cut quartz crystal with a 10 mm diameter gold electrode (QSX301 − Standard Gold) with a fundamental resonance frequency of 5 MHz from Q-Sense AB, Västra Frölunda, Sweden.

Prior to each experiment, the gold sensor surface upon the quartz crystals was cleaned with piranha solution (70% sulfuric acid and 30% hydrogen peroxide) for 3 min, 40% w/v sodium hydroxide solution for 3 min, and subsequently twice with piranha solution for 3 min. After each cleaning step, crystals were rinsed twice with deionized water and dried with nitrogen gas. Sensors were transferred to the QCM, and the system was equilibrated with deionized water at 23.35 ± 0.025 °C. Once all resonant overtone parameters were within the range stipulated by the manufacturer, the system was pre-equilibrated with K-medium lacking cells, the f and D were re-established in the new

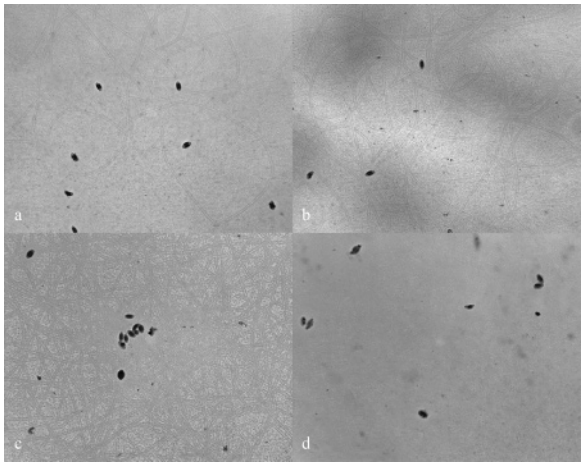

Figure 3. (a−d) Time-course study of trail formation for *A. coffeaeformis*: 30 min (a); 60 min (b); 4 h (c); 20 h (d).

experimental medium, and the system was allowed to stabilize prior to the introduction of cells. K-medium with cells was briefly injected into the instrument flow cell "loop" to allow for temperature stabilization, and thereafter approximately 0.4 mL of K-medium with suspended cells was introduced to the measurement chamber. Data collected from the third overtone were used for data analysis in all experiments.

After each experiment, the QCM sensor was removed and immediately fixed in K-medium with 2.5% gluteraldehyde (Sigma-Aldrich). To allow microscopic investigation of the sensor surface, an 11 mm diameter O-ring was placed upon a standard microscope slide, and the internal "reservoir" was filled with K-medium. The QCM sensor was then inverted and placed upon the O-ring. Images were taken along a predetermined axis from a significant point upon the crystal, comprising four sample paths of 0°, 45°, 90°, and 135° from the point of origin, with all paths passing through the electrode center and spanning the electrode diameter (Figure 2b). Images were taken using a Panasonic digital 3CCD camera set upon a Leica inverted DMIL microscope, and images were recorded using a Pioneer rewritable video disk recorder (VDR − V1000P). Cells within the sample data set were counted (the central node counted only once), and an estimate of the total cell concentration on the electrode surface was made.

Results and Discussion

Time-Dependent Study of Cellular Adhesion and Surface Modification. The mucilaginous trails deposited by the fouling diatoms *A. coffeaeformis* and *C. australis* were successfully imaged using the dye Stains All (0.1 g in 100 mL of formamide). Rather than the dye staining the trail material in the standard fashion (i.e., interacting with the organic material to yield a color change), a blue precipitate produced via the mixing of the dye with seawater media was found to strongly adhere to the trails, revealing fine structural details. Trail production observed for *A. coffeaeformis* over a 20 h period (Figure 3a−d) illustrates the rapid rate of surface modification possible from very few adhered diatoms upon a surface (~1631 cells/78.5 mm^2). Trail material is well established after 30 min on the substrate surface (Figure 3a), consistent with microscopic observations revealing that cellular motility commences immediately upon initial adhesion. Within 4 h, EPS has accumulated to cover significant areas of the surface (Figure 3c), and by 20 h, the native glass substrate has been completely covered (Figure 3d).

The three-dimensional structure of these trails was observed at high magnification using reflection mode SLCM (Figure 4). The physical structure of the trails deposited by *A. coffeaeformis* includes two parallel trails that are each produced by an independent raphe contacting the surface during motility (Figure 4a). This feature is unique to this group, given that pennate diatom morphology predominantly allows for a sole raphe (the driving raphe) to be contacting the surface at any given time. The visualized heights of the "stained" trails extended up to 1 μm from the slide surface (Figure 4b).

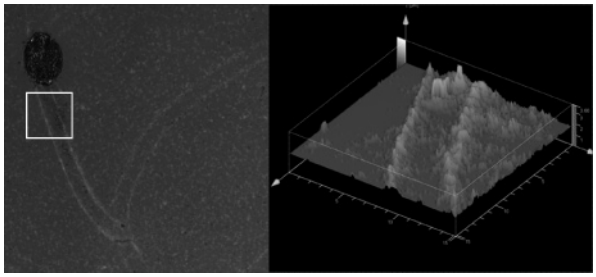

Figure 4. (a) Reflection mode SLCM image of *A. coffeaeformis* mucilaginous trail. (b) Three-dimensional high-magnification reflection mode image of *A. coffeaeformis* trail.

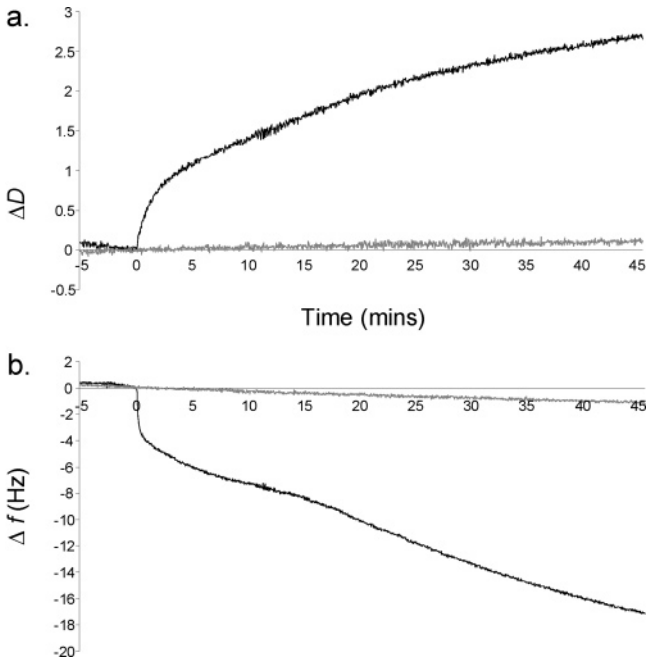

Figure 5. The dissipation (a) and frequency (b) responses recorded over a 45 min period for K-medium (gray) and ~15 653 *A. coffeaeformis* cells (black); cells introduced to QCM chamber at time 0. Data sets fitted to intercept 0 at $t = 0$ to allow comparative analysis.

Measurement of Initial Cellular Adhesion and Surface Modification of *A. coffeaeformis* Using QCM. In Figure 5, a representative QCM response produced by ~15 653 adhered *A. coffeaeformis* cells is compared to baseline data produced by sterile K-medium devoid of cells. *A. coffeaeformis* is used as an example here as QCM data can be correlated easily to the aforementioned EPS staining studies. Prior to the introduction of cells, the QCM was equilibrated in K-medium without cells for 10 min, whereupon cells were introduced to the QCM chamber in the same medium as was used to achieve the baseline curve, and therefore the QCM response can be attributed to the interactions between the cells and the gold electrode only.

Immediately upon the introduction of cells to the QCM chamber, a sharp *f* decrease and *D* increase is recorded (Figure 5). Previous studies employing mammalian cells have established that only cells that exhibit specific-integrin mediated adhesion, rather than those loosely interacting with the electrode surface, impact significantly upon recordable parameters,[29] and,

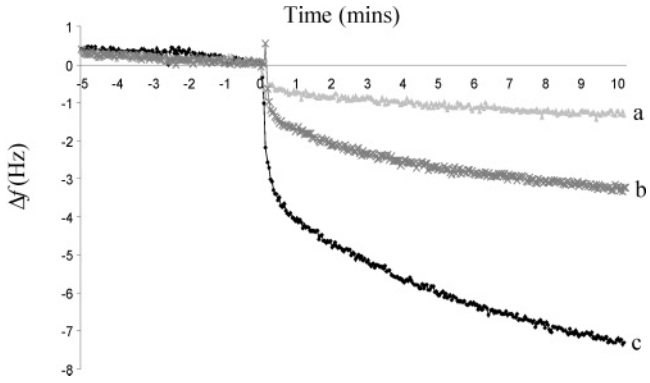

Figure 6. Frequency responses recorded upon the introduction ($t = 0$) of varied concentrations of *A. coffeaeformis* to the QCM chamber ((a) ~537 cells, (b) ~1758 cells, (c) ~15 653 cells).

coupled with the point of injection and the nominal cell sedimentation distance (≤0.2−0.4 mm), we attribute the immediate *f* and *D* responses to cells contacting and adhering to the substrate surface. Unlike mammalian cells that have been described as requiring substantial time to form strong adhesion complexes with the substrate,[42] an advantage, and indeed a cornerstone of diatom success, is their ability to employ EPS to quickly adhere to a given substrate. The magnitude of the initial *f* shift upon cell adhesion was found to be cell concentration dependent, where Δf values of −3.5, −1.3, and −0.6 Hz were recorded for ~15 653, ~1758, and ~537 cells, respectively (Figure 6). Proportional frequency responses relative to the number of cells seeded upon the crystal surface are well established in other systems using considerably greater numbers of mammalian cells,[20,22,24,27] with cell-induced Δf and ΔD values recorded with as few as 70−80 monkey kidney epithelial (MKE) cells.[19] Although the adhesion of ~537 cells provided significant *f* and *D* responses, experiments employing much larger cell concentrations achieved far more consistent results over the experimental time course (20 h), and therefore only those are discussed in detail hereafter.

Directly following the initial sharp *f* response, *f* continues to gradually decrease, becoming more negative over the entire course of the experiment, concluding at −39 Hz at 20 h (Figure 7b). Comparatively, *D* values logarithmically increase after initial adhesion, ultimately to a value of 6.6 (Figure 7a). These parameter responses are far greater than those seen for the K-medium baseline, where maximum Δf and ΔD values of −6.8 Hz and 0.4 were recorded at 20 h (Figure 7a,b). Although these baseline parameter readings are within the acceptable factory set range (Δf of 1.5 Hz and ΔD of 0.2 per hour), separate experiments found that the shift observed when the sensor crystal was in contact with K-medium was approximately twice that when in contact with deionized water (data not shown).

The morphology of *A. coffeaeformis*, and indeed other diatom species including *C. australis*, includes an outer hard silica frustule, preventing any cell morphological alterations, and therefore cell plasticity has no role in post-adhesion parameter responses. This is unlike work on other living cells, including those on bovine endothelial cells, where post adhesion Δf and ΔR were correlated to alterations in cell cytoskeletal architecture, allowing cells to modify their morphology and spread upon the electrode surface.[21] We propose the post-adhesion *f* and *D* responses here are derived from the deposition of adhesive EPS on the substrate surface as a result of cellular motility. As we have previously illustrated (Figure 3), EPS secreted by cells during motility commences soon after initial adhesion, rapidly covering substantial areas of the substrate. This time-dependent

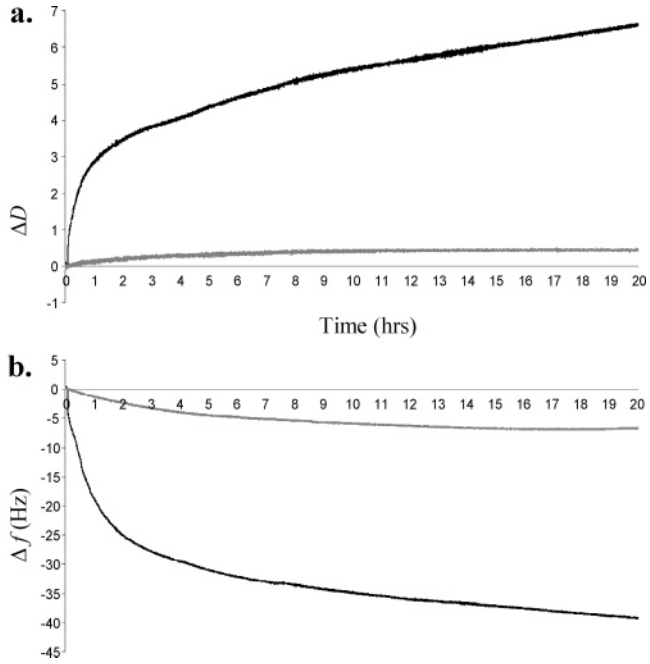

Figure 7. Dissipation (a) and frequency (b) responses recorded for K-medium (gray) and *A. coffeaeformis* (black) over a 20 h period (post cell-inoculation).

deposition of adhesive EPS on the surface is recorded as an increase in the measure of the adsorbed mass, *f*, and subsequently an increase in energy dissipated at the solution−surface interface, *D*. The greatest parameter responses are evident during the initial 3 h post-injection, during which time much of the virgin electrode surface is covered with EPS, and thereafter slowly tapering, presumably as a function of the available electrode area for EPS "colonization", rather than motility. As photosynthetic organisms, it is a consideration that results may become unreliable after 10 h post-inoculation as cells anticipate the commencement of the "day" phase of their light cycle. Parallel experiments reveal motility continues for hours during this prolonged dark period (data not shown), and Smith and Underwood[43] have reported that diatoms can produce various EPS's, sometimes in varied forms, for up to 3 days in the dark. We also tested for recordable responses dependent upon the time of introduction to the QCM chamber relative to their daily light/dark cycle. It was established that cells introduced to the QCM at the commencement of their dark cycle induced *f* and *D* responses equivalent to those of cells introduced during their light cycle (data not shown).

We further conclude that, along with an absence of any cell morphological alterations upon adhesion, it is unlikely that the actual cellular mass contributes substantially to the data presented. As illustrated in Figure 4, the adhesive mucilage secreted from the cell raphe during cellular adhesion and motility elevates the cell upon an adhesive trail, effectively displacing the cell from the surface. Consequently, only a fraction of the actual cellular mass is likely to be exposed within the instrument detection limits (0.25 μm at 20 °C in water).[44] Furthermore, unlike previous studies that describe a cellular monolayer forming upon the substrate surface, diatoms occupy only a negligible portion of the available substrate area (~2.8% for ~15 653 *A. coffeaeformis* cells). Because we have demonstrated the likelihood that much, if not all, of the vacant area is to be covered with EPS after significant incubation periods, the actual cellular mass within range of instrument detection limits is unlikely to contribute substantially to the overall signal recorded.

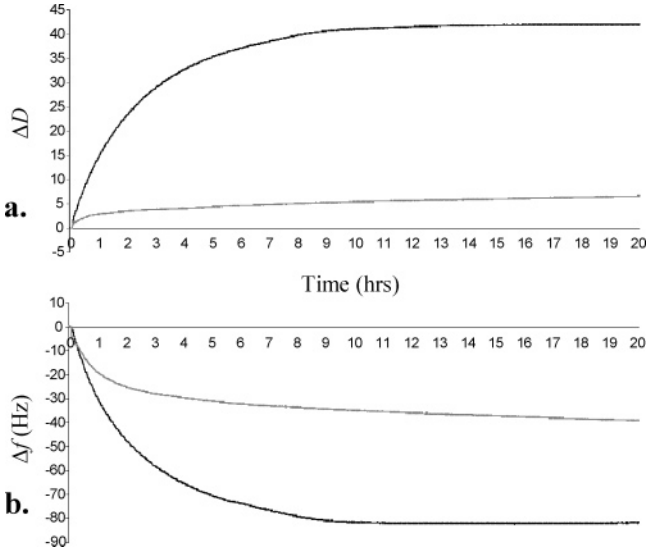

Figure 8. Dissipation (a) and frequency (b) responses produced by ~15 653 *A. coffeaeformis* (gray) and ~16 480 *C. australis* (black) cells over a 20 h time course.

Therefore, we are effectively able to measure interactions between cellular EPS and the substrate in-situ and in real-time.

Measuring the Interactions between Cellular-Derived EPS and the Substrate Surface from Two Fouling Diatom Species. We utilized the QCM to compare the interactions between cellular EPS and the gold electrode surface from the two diatom species *C. australis* and *A. coffeaeformis*. Figure 8 reveals typical results from time-course experiments where comparable numbers of *A. coffeaeformis* (~15 653) and *C. australis* (~16 480) were seeded upon the electrode surface. Upon initial adhesion, both *A. coffeaeformis* and *C. australis* demonstrate a gradual reduction in frequency and logarithmic increase in dissipation. For *A. coffeaeformis*, this trend continued for the entire duration of the 20 h experimental period; however, f and D values for *C. australis* reach a ceiling at ~15 h, illustrating little variation for the rest of the experiment. The magnitude of the f and D responses differed considerably between cell types. *C. australis* induced larger f and D responses, −82 Hz and 42, respectively, as compared to those for *A. coffeaeformis* ($\Delta f = -32$ Hz, $\Delta D = 6.6$). The disparity between the frequency outputs produced from each species is likely because of differences in the effective EPS mass deposited upon the surface. We propose this can be attributed to the relative motility rates of each species. Previous studies have found a greater proportion of *C. australis* cells remain motile post-inoculation upon a surface as compared to *A. coffeaeformis*,[38] and our own microscopic investigations clearly illustrate *C. australis* to exhibit a far greater speed of motility than that of *A. coffeaeformis* (data not shown). Consequently, *C. australis* achieves a greater rate of EPS deposition upon the surface, and therefore the larger f response over the duration of the experiment. This is also likely to account for the "ceiling" effect illustrated in the *C. australis* data at approximately 15 h post-inoculation. Because of an increased rate of motility, *C. australis* deposits far more material at a rapid rate, eventually saturating the electrode surface, and therefore the detectable range of the instrument. In support of this point, the phenomenon was not demonstrated in *A. coffeaeformis* experiments that utilized a lower cell concentration (data not shown).

The viscoelastic properties of the adhered EPS layers from both species were analyzed via a $\Delta f/\Delta D$ plot (Figure 9).[19] We found that, following initial cell contact and adhesion to the surface, the viscoelastic properties of the *C. australis* adlayer remained remarkably constant. In contrast, *A. coffeaeformis* exhibited variation in the viscoelastic response of the adlayer that was reproduced in several experiments. The generally linear relationship exhibited between f and D for both species reveals no considerable conformational changes within the adlayer over time, therefore indicating a lack of cross-linked-mediated adhesion that is evident in other studied marine biological adhesives.[32] When compared to the baseline data, the overwhelming cellular contribution to both of the parameter outputs is evident, much of this during the initial 2 h post-inoculation (Figure 9). The differences between the cell types illustrated in the $\Delta f/\Delta D$ plot can be further expressed as a function of time (Figure 10). The $\Delta f/\Delta D$ ratio exhibited for each species was replicated several times, revealing "signature" $\Delta f/\Delta D$ values unique to each species type (~2 for *C. australis* and ~6 for *A. coffeaeformis*). We propose the distinction between the QCM responses recorded for the EPS of each species is likely the product of the nature of the interaction between the EPS and the electrode surface, and/or differences between the actual physical properties of the EPS adlayer.

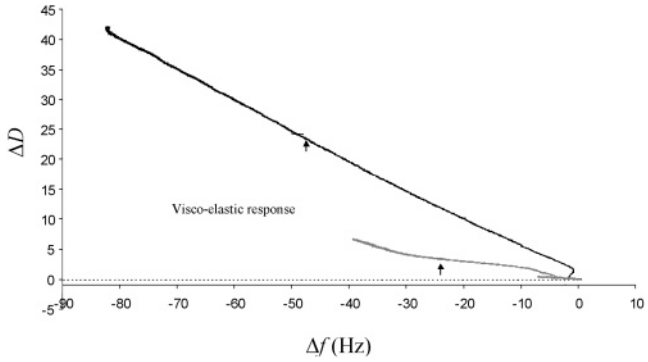

Figure 9. $\Delta f/\Delta D$ plot over a 20 h time course for *C. australis* (black), *A. coffeaeformis* (gray), and K-medium (light gray). Arrows indicate 2 h post-inoculation.

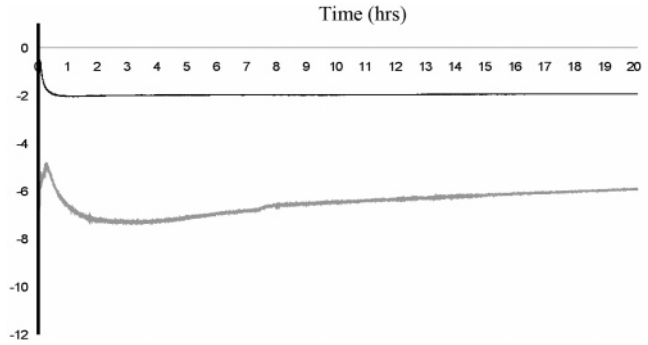

Figure 10. Plot of Δf (Hz)/ΔD for *A. coffeaeformis* (grey) and *C. australis* (black) during a 20 h time course.

Because little is known of the chemical composition of diatom EPS, it has not been possible at this stage for researchers to meaningfully compare the EPS secreted from species of different fouling ability and therefore determine whether cell morphology or EPS composition plays the principal role in determining diatom fouling potential. However, a number of studies have investigated the strength of adhesion of various diatom species on a range of surfaces and/or in dynamic flow environments.[37,38,45,46] Holland et al.[38] compared three diatom species, including *C. australis* and *A. coffeaeformis var. perpusilla* (Grunow), where rates of motility and strength of adhesion were compared for different silicon elastomer surfaces. The researchers reported the wall shear forces required to dislodge cells from

both acid-washed glass and hydrophobic poly(dimethylsiloxane) elastomer (PDMSE) were consistently greater for *A. coffeaeformis*, while both species adhered more strongly to the PDMSE than glass. Because we have demonstrated a clear distinction between the EPS properties as ascertained from QCM analysis of two diatom species of significantly different fouling potential, we propose our data may signal that EPS plays the significant role in determining the success of diatom species in fouling.

Conclusion

Of the estimated 10 000 diatom species in the ocean, it is significant that only some 8−10 species have been reported to contribute substantially to the biofouling of submerged artificial surfaces. Although a number of techniques have yielded important results regarding diatom strength of adhesion on a range of substrate surfaces, it has proved difficult to establish the relative contributions that cell morphology and the physical and chemical properties of the EPS make in determining cell adhesion strength. Here, we have utilized QCM-D to measure the time-dependent deposition of adhesive EPS on the substrate surface via Δf, along with the viscoelastic properties of the adlayer via ΔD. Parameter shifts illustrated for *C. australis* (−82 Hz Δf and 42 ΔD) were proportionally greater than those for *A. coffeaeformis* (−32 Hz Δf and 6.6 ΔD) where comparable cell concentrations were seeded upon the QCM sensor over a 20 h time-course. Subsequent data analysis by way of a $\Delta f/\Delta D$ plot enabled us to characterize the mechanical properties of the EPS produced by each species, where ratios of ∼2 and ∼6 for *C. australis* and *A. coffeaeformis*, respectively, reveal key differences in the relative EPS viscoelastic properties that may correlate to the reported fouling abilities of the two species.

Acknowledgment. We thank John Lewis from DSTO for valuable discussions and technical support. The Australian Research Council and our industry partner Akzo Nobel, Gateshead, UK, provided funding (Industry Linkage grant number LP0454982). We also thank the Defence Science and Technology Organization (DSTO) of the Australian Department of Defence for financial assistance.

References and Notes

(1) O'Sullivan, C. K.; Guilbault, G. G. Commercial quartz crystal microbalances − theory and applications. *Biosens. Bioelectron*. **1999**, *14*, 663−670.
(2) Marx, K. A. Quartz Crystal Microbalance: A useful tool for studying thin polymer films and complex biomolecular systems at the solution-surface interface. *Biomacromolecules* **2003**, *4*, 1099−1120.
(3) Sauerbury, G. *Z. Phys.* **1959**, *155*, 206−222.
(4) King, W. H. Piezoelectric sorption detector. *Anal. Chem.* **1964**, *36*, 1735−1739.
(5) Nomura, T.; Okuhara, M. Frequency shifts in piezoelectric quartz crystals immersed in organic liquids. *Anal. Chim. Acta* **1982**, *142*, 281−284.
(6) Kurosawa, S.; Tawara, E.; Kamo, N.; Kobatake, Y. Oscillating frequency of piezoelectric quartz crystal in solutions. *Anal. Chim. Acta* **1990**, *230*, 41−49.
(7) Bruckenstein, S.; Shay, M. An in situ weighing study of the mechanism for the formation of the adsorbed oxygen monolayer at the gold electrode. *J. Electroanal. Chem.* **1985**, *188*, 131−136.
(8) Benje, M.; Eierman, M.; Pittermann, U.; Weil, K. G. An improved quartz crystal microbalance. Applications to the electrocrystallization and dissolution of nickel. *Ber. Bunsen-Ges. Phys. Chem.* **1986**, *90*, 435−439.
(9) Thompson, M.; Arthur, C. L.; Dhaliwal, G. K. Liquid-phase piezoelectric and acoustic transmission studies of interfacial immunochemistry. *Anal. Chem.* **1986**, *58*, 1206−1209.
(10) Guilbault, G. G.; Hock, B.; Schmid, R. PZ immunosensor of atrazine in drinking water. *Biosens. Bioelectron*. **1992**, *7*, 411−419.
(11) Nakanashi, K.; Muguruma, H.; Karube, I. A novel method of immobilizing antibodies on a quartz crystal microbalance using plasma-polymerized films for immunosensors. *Anal. Chem.* **1996**, *68*, 1695−1700.
(12) Nivens, D. E.; Chambers, J. Q.; Anderson, T. R.; White, D. C. Long-term, on-line monitoring of microbial films using a quartz crystal microbalance. *Anal. Chem.* **1993**, *65*, 65−69.
(13) Gryte, D. M.; Ward, M. D.; Hu, W. Real-time measurement of anchorage dependent cell adhesion using a quartz crystal microbalance. *Biotechnol. Prog.* **1993**, *9*, 105−108.
(14) Redepenning, J.; Schlesinger, T. K.; Mechalke, E. J.; Puleo, D. A.; Bizios, R. Osteoblast attachment monitored with a quartz crystal microbalance. *Anal. Chem.* **1993**, *65*, 3378−3381.
(15) Rodahl, M.; Höök, F.; Krozer, A.; Brzezinski, P.; Kasemo, B. Quartz crystal microbalance setup for frequency and Q-factor measurements in gaseous and liquid environments. *Rev. Sci. Instrum.* **1995**, *66*, 3924−3930.
(16) Rodalh, M.; Höök, F.; Kasemo, B. QCM operation in liquids: An explanation of measured variations in frequency and Q factor with liquid conductivity. *Anal. Chem.* **1996**, *68*, 2219−2227.
(17) Rodahl, M.; Kasemo, B. A simple setup to simultaneously measure the resonant frequency and the absolute dissipation factor of a quartz crystal microbalance. *Rev. Sci. Instrum.* **1996**, *67*, 3238−3241.
(18) Rodahl, M.; Höök, F.; Fredriksson, C.; Keller, C. A.; Krozer, A.; Brzezinski, P.; Voinova, M.; Kasemo, B. Simultaneous frequency and dissipation factor QCM measurements of biomolecular adsorption and cell adhesion. *Faraday Discuss.* **1997**, *107*, 229−246.
(19) Fredriksson, C.; Kihlman, M.; Rodahl, M.; Kasemo, B. The piezoelectric quartz crystal mass and dissipation sensor: A means of studying cell adhesion. *Langmuir* **1998**, *14*, 248−251.
(20) Wegener, J.; Janshoff, A.; Galla, H. Cell adhesion monitoring using a quartz crystal microbalance: comparative analysis of different mammalian cell lines. *Eur. Biophys. J.* **1998**, *28*, 26−37.
(21) Zhou, T.; Marx, K. A.; Warren, M.; Schulze, H.; Braunhut, S. J. The quartz crystal microbalance as a continuous monitoring tool for the study of endothelial cell surface attachment and growth. *Biotechnol. Prog.* **2000**, *16*, 268−277.
(22) Marxer, C. G.; Coen, M. C.; Bissig, H.; Greber, U. F.; Schlapbach, L. Simultaneous measurement of the maximum oscillation amplitude and the transient decay time constant of the QCM reveals stiffness changes in the adlayer. *Anal. Bioanal. Chem.* **2003**, *377*, 570−577.
(23) Marxer, C. G.; Coen, M. C.; Greber, T.; Greber, U. F.; Schlapbach, L. Cell spreading on quartz crystal microbalance elicits positive frequency shifts indicative of viscosity changes. *Anal. Bioanal. Chem.* **2003**, *377*, 578−586.
(24) Marx, K. A.; Zhou, T.; Warren, M.; Braunhut, S. J. Quartz crystal microbalance study of endothelial cell number dependent differences in initial adhesion and steady-state behaviour: evidence for cell − cell cooperativity in initial adhesion and spreading. *Biotechnol. Prog.* **2003**, *19*, 987−999.
(25) Lüthgens, E.; Herrig, A.; Kastl, K.; Steinem, C.; Reiss, B.; Wegener, J.; Pignataro. B.; Janshoff, A. Adhesion of liposomes: a quartz crystal microbalance study. *Meas. Sci. Technol.* **2003**, *14*, 1865−1875.
(26) Jenkins, M. S.; Wong, K. C. Y.; Chhit, O.; Bertram, J. F.; Young, R. J.; Subaschandar, N. Quartz crystal microbalance-based measurements of shear-induced senescence in human embryonic kidney cells. *Biotechnol. Bioeng.* **2004**, *88*, 392−398.
(27) Li, J.; Thielemann, C.; Reuning, U.; Johannsmann, D. Monitoring of integrin-mediated adhesion of human ovarian cancer cells to model protein surfaces by quartz crystal resonators: evaluation in the impedance analysis mode. *Biosens. Bioelectron.* **2005**, *20*, 1333−1340.
(28) Marx, K. A.; Zhou, T.; Montrone, A.; Schulze, H.; Braunhut, S. J. A quartz crystal microbalance cell biosensor: detection of microtubule alterations in living cells at nM nocodazole concentrations. *Biosens. Bioelectron.* **2001**, *16*, 773−782.
(29) Wegener, J.; Seebach, J.; Jansoff, A.; Galla, H. Analysis of the composite response of shear wave resonators to the attachment of mammalian cells. *Biophys. J.* **2000**, *78*, 2821−2833.
(30) Höök, F.; Kasemo, B. Variations in coupled water, viscoelastic properties, and film thickness of Mefp-1 protein film during adsorption and cross-linking: a quartz crystal microbalance with dissipation monitoring, ellipsometry, and surface plasmon resonance study. *Anal. Chem.* **2001**, *73*, 5796−5804.

(31) Fant, C.; Elwing, H.; Höök, F. The influence of cross-linking on protein − protein interactions in a marine adhesive: the case of two byssus plaque proteins from the blue mussel. *Biomacromolecules* **2002**, *3*, 732−741.
(32) Berglin, M.; Delage, L.; Potin, P.; Vilter, H.; Elwing, H. Enzymatic cross-linking of a phenolic polymer extracted from the marine alga *Fucus serratus*. *Biomacromolecules* **2004**, *5*, 2376−2383.
(33) Edgar, L. A.; Picket-Heaps, J. D. Diatom locomotion. *Prog. Phycol. Res.* **1984**, *3*, 47−84.
(34) Hoagland, K. D.; Rosowsk, J. R.; Gretz, M. R. Review: Diatom extracellular polymeric substances: function, fine structure, chemistry and physiology. *J. Phycol.* **1993**, *29*, 537−566.
(35) Wetherbee, R.; Lind, J. L.; Burke, J.; Quatrano, R. S. The first kiss: establishment and control of initial adhesion by raphid diatoms. *J. Phycol.* **1998**, *34*, 9−15.
(36) Wigglesworth-Cooksey, B.; van der Mei, H.; Busscher, H. J.; Cooksey, K. E. The influence of surface chemistry on the control of cellular behaviour: studies with a marine diatom and a wettability gradient. *Colloids Surf., B* **1999**, *15*, 71−79.
(37) Finlay, J. A.; Callow, M. E.; Ista, L. K.; Lopez, G. P.; Callow, J. A. The influence of surface wettability of the adhesion strength of settled spores of the green alga *Enteromorpha* and the diatom *Amphora*. *Integr. Comp. Biol.* **2002**, *42*, 1116−1115.
(38) Holland, R.; Dugdale, T. M.; Wetherbee, R.; Brennan, A. B.; Finlay, J. A.; Callow, J. A.; Callow, M. E. Adhesion and motility of fouling diatoms on a silicone elastomer. *Biofouling* **2004**, *20*, 323−329.
(39) Higgins, M. J.; Crawford, S. A.; Mulvaney, P.; Wetherbee, R. Characterization of the adhesive mucilages secreted by live diatom cells using atomic force microscopy. *Protist* **2002**, *153*, 25−38.
(40) Higgins, M. J.; Molino, P.; Mulvaney, P.; Wetherbee, R. The structure and nanomechanical properties of the adhesive mucilage that mediates diatom-substratum adhesion and motility. *J. Phycol.* **2003**, *39*, 1181−1193.
(41) Anderson, R. A.; Jacobsen, D. M.; Sexton, J. P. *Provasoli Guillard centre for culture of marine phytoplankton − catalogue of strains*; West Boothbay Harbour, Maine, 1991; 98 pp.
(42) Sagvolden, G.; Giaever, I.; Pettersen, E. O.; Feder, J. Cell adhesion force microscopy. *Proc. Natl. Acad. Sci. U.S.A.* **1999**, *96*, 471−476.
(43) Smith, D. J.; Underwood, G. J. C. The production of extracellular carbohydrates by estuarine benthic diatoms: the effects of growth phase and light and dark treatment. *J. Phycol.* **2000**, *36*, 321−333.
(44) Kanazawa, K. K.; Gordon, J. G. Frequency of a quartz crystal microbalance in liquid. *Anal. Chem.* **1985**, *57*, 1770−1771.
(45) Bishop, J. H.; Silva, S. R.; Silva, V. M. A study of microfouling on antifouling coatings using electron microscopy. *J. Oil Colour Chem. Assoc.* **1974**, *57*, 30−35.
(46) Pyne, S.; Fletcher, R. L.; Jones, E. B. G. Attachment studies on three common fouling diatoms. *Int. Congr. Mar. Corros. Fouling* **1984**, *6*, 325−346.

BM0605661